

# A SPHERICAL ELECTRO-OPTIC HIGH-VOLTAGE SENSOR

M. C. McKinley, C. V. Smith, Jr., W. C. Nunnally

Center for Energy Conversion Research, University of Texas at Arlington, P.O. Box 19380, Arlington, Texas 76019

R. Magnusson

Electrical Engineering Department, University of Texas at Arlington, P.O. Box 19016, Arlington, Texas 76019

T. D. Black

Physics Department, P.O. Box 19059, University of Texas at Arlington, Arlington, Texas 76019

## Abstract

A spherical electro-optic (EO) crystal is introduced for photonic measurement of pulsed high-voltage fields. A spherical shape is used in order to reduce electric field gradients in the vicinity of the sensor. The sensor is pure dielectric and is interrogated remotely using a laser. The sensor does not require the connection of any conducting components, which results in the highest electrical isolation. The spherical nature of the crystal coupled with the incident laser beam, and crossed polarizers (intensity modulation scheme), automatically produces interference figures. The fringes move with the application of an electric field applied to the EO crystal, and a photodetector senses the pattern movement. The sensor can be made small (e.g. < 3mm diam.) resulting in a large AC bandwidth, (e.g. > 4 GHz). Proof of principle results are presented for the use of a solid sphere (~3 mm diam.) of LiNbO<sub>3</sub> for measuring pulsed electric and voltage fields.

## Introduction

As part of a continued support program for the SDI Space Power Experiments Aboard Rockets (SPEAR) projects, the University of Texas at Arlington Center for Energy Conversion Research (UTA/CECR) has initiated a research effort<sup>1,2</sup> to determine the optimum high-voltage (HV) measurement technique for space. Based on results obtained by many researchers over the years since 1956<sup>3</sup>, measurements based on the EO effect, and Senarmont optical arrangements,<sup>4</sup> have definite advantages over conventional non-optical techniques [e.g. large bandwidth (BW), compact size, low weight, pure dielectric configurations are possible, fiber optic compatibility, excellent electrical isolation, better immunity to EMI/EMP, wide range of application (static to microwaves) and well established by many researchers]. In an effort to expand the collection of available knowledge concerning EO sensors, a new EO HV measurement technique is introduced based on  $\vec{E}$  induced irradiance,  $I$ , amplitude modulation (AM) of finite features (e.g. melatopes, isogyres, isochromes, etc.<sup>5</sup>) of EO interference figures (IFs).  $\vec{E}$  modulated c-axis IFs have been demonstrated using both monochromatic non-coherent IFs<sup>4</sup>, and laser IFs (LIFs)<sup>6</sup> of uniaxial, box geometry EO crystals. The new technique is demonstrated for pulsed voltage and  $\vec{E}$  measurements using a new type of sensor consisting of a solid sphere of uniaxial EO crystal.<sup>7</sup> To our knowledge, neither a HV or  $\vec{E}$  measurement method based on finite features of IFs or LIFs, nor a spherical EO sensor (SEOS) has been reported by other researchers. The SEOS is 100% dielectric, optically coupled (maximum electrical isolation), and passive. The spherical geometry, coupled with a TEM<sub>00</sub> laser beam, automatically results in an inherent LIF HV measurement technique. Since a finite LIF is used, the conventional  $\lambda/4$  plate (maximum sensitivity, linearity, and  $\vec{E}$  or V polarity determination) is eliminated, and an infinite distribution of LIF quiescent (Q) points (position in IF or LIF where sensing aperture,  $\Sigma$ , is located) are available simultaneously, as are many values of half-wave voltage,  $V_{\pi}$ . Hence, an infinite number of sensing orientations are possible with a single sensor, not just transverse and longitudinal. Other reasons for studying the spherical geometry include: spherical symmetry simplifies analysis; a uniform  $\vec{E}$  exists within a spherical dielectric when immersed in a uniform  $\vec{E}$ ; conoscopic light production in a crystal (necessary condition for producing an IF or LIF) is achieved automatically without the use of condensing and auxiliary lenses,<sup>5</sup> and the spherical geometry has important consequences concerning sensor presence on breakdown phenomena in HV systems.<sup>7</sup> This research has also led to advances in the optical characterization of crystals.<sup>8</sup>

## Conventional EO Sensors

Conventional AM EO sensors (Fig. 1) mostly employ box or

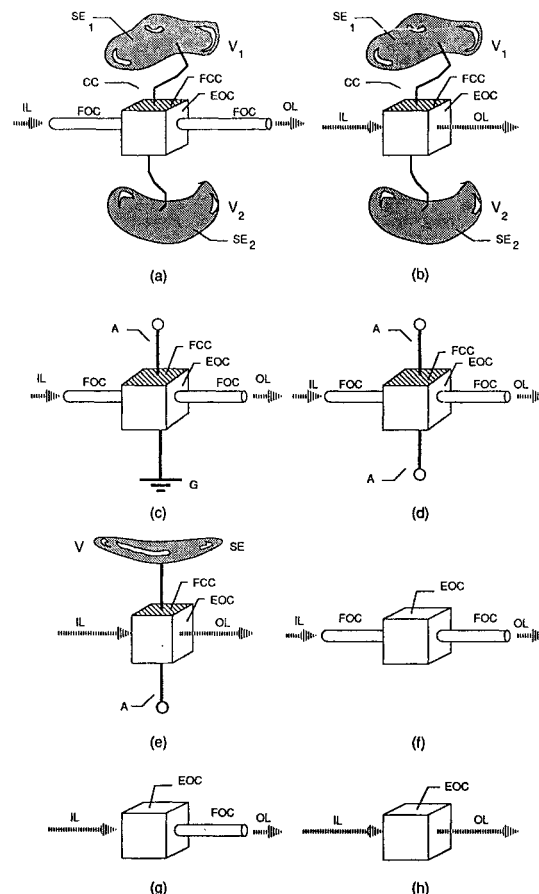


Fig. 1. Conventional EO HV and  $\vec{E}$  sensor configurations. Conductor coupled: guided (a)<sup>9,10</sup> and unguided (b)<sup>3,4,11</sup> light coupling. Antenna coupled: guided (c),<sup>12</sup> (d)<sup>13,14</sup> and unguided (e)<sup>15</sup> light coupling. Dielectric coupled (pure dielectric): guided (f),<sup>16,17,18,19</sup> partial guided (g)<sup>20</sup> and unguided (h)<sup>21,22</sup> light coupling. For ease of illustration, a transverse configuration is shown for all sensors using conductors. For longitudinal sensors, thin film conductive coatings are used. Close proximity optical (e.g. lenses, prisms, etc.), electrical, and hardware components are also used for some sensors. FOC: fiber optic cable; CC: conducting coupler; IL: incident light; FCC: field coupling-concentrating conductor; EOC: EO crystal; OL: output light; SE: source electrode; V: source electrode potential; A: conducting antenna; G: ground.

cylindrical geometry crystals. Some configurations have conducting components (provide a concentrated, uniform  $\vec{E}$  in the crystal), and others are pure dielectric. Hitherto, the effect of geometry on EO HV and  $\vec{E}$  sensors has largely concerned sensor optics, not the effect of sensor geometry and material on HV systems, and the effect of HV breakdown phenomena on HV EO sensors. Also neglected is the useful operating range of the sensor with respect to the HV environment.

## Operating Regions

Four  $\vec{E}$  related characteristics may be used to define an operating region for an EO sensor: (1) breakdown, (2) sensitivity, (3) linearity and (4)

Report Documentation Page				Form Approved OMB No. 0704-0188	
Public reporting burden for the collection of information is estimated to average 1 hour per response, including the time for reviewing instructions, searching existing data sources, gathering and maintaining the data needed, and completing and reviewing the collection of information. Send comments regarding this burden estimate or any other aspect of this collection of information, including suggestions for reducing this burden, to Washington Headquarters Services, Directorate for Information Operations and Reports, 1215 Jefferson Davis Highway, Suite 1204, Arlington VA 22202-4302. Respondents should be aware that notwithstanding any other provision of law, no person shall be subject to a penalty for failing to comply with a collection of information if it does not display a currently valid OMB control number.					
1. REPORT DATE <b>JUN 1989</b>		2. REPORT TYPE <b>N/A</b>		3. DATES COVERED <b>-</b>	
4. TITLE AND SUBTITLE <b>A Spherical Electro-Optic High-Voltage Sensor</b>				5a. CONTRACT NUMBER	
				5b. GRANT NUMBER	
				5c. PROGRAM ELEMENT NUMBER	
6. AUTHOR(S)				5d. PROJECT NUMBER	
				5e. TASK NUMBER	
				5f. WORK UNIT NUMBER	
7. PERFORMING ORGANIZATION NAME(S) AND ADDRESS(ES) <b>Center for Energy Conversion Research, University of Texas at Arlington, P.O. Box 19380, Arlington, Texas 76019</b>				8. PERFORMING ORGANIZATION REPORT NUMBER	
9. SPONSORING/MONITORING AGENCY NAME(S) AND ADDRESS(ES)				10. SPONSOR/MONITOR'S ACRONYM(S)	
				11. SPONSOR/MONITOR'S REPORT NUMBER(S)	
12. DISTRIBUTION/AVAILABILITY STATEMENT <b>Approved for public release, distribution unlimited</b>					
13. SUPPLEMENTARY NOTES <b>See also ADM002371. 2013 IEEE Pulsed Power Conference, Digest of Technical Papers 1976-2013, and Abstracts of the 2013 IEEE International Conference on Plasma Science. Held in San Francisco, CA on 16-21 June 2013. U.S. Government or Federal Purpose Rights License.</b>					
14. ABSTRACT <b>A spherical electro-optic (EO) crystal is introduced for photonic measurement of pulsed high-voltage fields. A spherical shape is used in order to reduce electric field gradients in the vicinity of the sensor. The sensor is pure dielectric and is interrogated remotely using a laser. The sensor does not require the connection of any conducting components, which results in the highest electrical isolation. The spherical nature of the crystal coupled with the incident laser beam, and crossed polarizers (intensity modulation scheme). automatically produces interference figures. The fringes move with the application of an electric field applied to the EO crystal, and a photodetector senses the pattern movement. The sensor can be made small (e.g. &lt; 3mm diam.) resulting in a large AC bandwidth, (e.g. &gt; 4 GHz). Proof of principle results are presented for the use of a solid sphere (-3 mm diam.) of LiNbO3 for measuring pulsed electric and voltage fields.</b>					
15. SUBJECT TERMS					
16. SECURITY CLASSIFICATION OF:			17. LIMITATION OF ABSTRACT <b>SAR</b>	18. NUMBER OF PAGES <b>4</b>	19a. NAME OF RESPONSIBLE PERSON
a. REPORT <b>unclassified</b>	b. ABSTRACT <b>unclassified</b>	c. THIS PAGE <b>unclassified</b>			

BW. The operating region may be defined by the particular combination of characteristics that exist within the region.  $\vec{E}$  may have amplitudes large enough such that breakdown phenomena (volume breakdown, surface flashover, etc.) may occur. If system breakdown is undesired, the presence of the EO sensor should not initiate breakdown. The EO sensor may or may not survive breakdown (designed or accidental) phenomena.  $\vec{E}$  may be such that no measurable response can be obtained from the EO sensor. If a measurable response can be obtained from the sensor, the linearity of the response will depend on the amplitude of the applied  $\vec{E}$  (assuming a linear Q-point) relative to  $V_{\pi}$ . The practical region of operation is one in which there is no breakdown (unless measurements associated with breakdown are desired), and sensitivity is sufficient to produce a measurable response that is linear. A sensor may survive larger amplitudes of  $\vec{E}$  by selection of geometry, and EO crystals with efficacious properties. By choosing a SEOS HV sensor, uniform  $\vec{E}$  measurement may be extended to larger amplitude regions of  $\vec{E}$  than for non-spherical geometries. The spatial characteristics of  $\vec{E}$  will determine if sensor BW is sufficient.

#### HV Environmental Considerations:

In order for an EO sensor to be successfully used in the HV environment, detrimental levels of both charged particle production and  $\vec{E}$  distortion (intensification) must be avoided. Charged particles in the HV environment may produce further  $\vec{E}$  distortion, measurement error, and breakdown. Both conductors and dielectrics influence the introduction of charged particles into a HV environment. Free electrons may be liberated from conductors via stable field emission at high values of  $\vec{E}$  ( $\sim 2 \times 10^9$  to  $\sim 5 \times 10^9$  Vm<sup>-1</sup>),<sup>23</sup> and photoelectrons may be liberated via energetic photons.  $\vec{E}$  distortion from conductors results from the presence of conduction band electrons. Dielectrics may distort  $\vec{E}$  in two ways. First, any dielectric material will have a finite electrical resistivity,  $\rho$ . Charge migration will then occur from an applied  $\vec{E}$  (especially where  $\partial\vec{E}/\partial t \neq 0$  and or  $\vec{E}$  may have large amplitude) and gather on the surface of the dielectric resulting in  $\vec{E}$  distortion. Secondly, EO crystals tend to have large values of permittivity,  $\epsilon$ , and undesirable  $\vec{E}$  may result from boundary conditions at dielectric interfaces.  $\vec{E}$  may be distorted enough for both dielectrics and conductors such that the operating point is driven above the Paschen curve resulting in breakdown phenomena (e.g. streamers, avalanching, corona, surface flashover, volume breakdown, catastrophic breakdown, etc.) between components of the HV system including the EO sensor. Sensors of Fig. 1 have two main problems: (1) conductive components, and (2) 90° edge geometries on both conductors and dielectrics. The smallest radius of curvature,  $R$ , determines the maximum  $\vec{E}$ - and  $V$ - fields for a given device. Small  $R$ 's at the 90° corners and edges of boxes and cylinders produce  $\vec{E}$  intensification > than that of a sphere. All other finite non-spherical geometries have minimum radii < than that of a sphere. Of the solid ellipsoidal dielectrics, when immersed in a uniform  $\vec{E}$ ,  $\vec{E}_0$ , only the sphere has a uniform internal  $\vec{E}$ ,  $\vec{E}_i$ , for any arbitrary orientation of the sphere, and provides the minimum  $\vec{E}$  intensification of any geometry. For an isotropic dielectric sphere immersed in an external medium and  $\vec{E}_0$ , volume breakdown occurs first in the medium with the smallest permittivity-breakdown strength product,  $\epsilon E_B$ . If  $\vec{E}_0$  is made large enough,  $\Delta V d^{-1} > E_B$ , initiating volume breakdown inside the sphere, where  $\Delta V$  is the maximum potential difference across the diameter,  $d$ , of the sphere. If  $d < \lambda_s$ , where  $\lambda_s$  is the wavelength of the highest spatial frequency component present in the modulating  $\vec{E}$  (time-varying or static), then the sphere may always be considered to be located in a uniform  $\vec{E}$  for practical purposes. The analytical solution for a static  $\vec{E}$ , both  $\vec{E}_i$  and external,  $\vec{E}_e$ , to an isotropic dielectric sphere in a uniform  $\vec{E}$ , is well known<sup>24</sup>.

#### Sensitivity and Linearity:

Sensitivity and linearity are both closely related by  $V_{\pi}$  and the Q-point. The % isochrome transmission,  $T$ , of the SEOS may be approximated by the  $T$  for conventional bulk AM EO sensors.<sup>25</sup> Since  $dT/dV \propto V_{\pi}^{-1}$ , then sensitivity may be increased by decreasing  $V_{\pi}$ . However,  $\delta V$ , the range of voltages over which the SEOS response is considered to be linear, is related to  $V_{\pi}$  by:  $\delta V = 0.6 V_{\pi}$ , where  $\delta V$  is arbitrarily determined by the 10% and 90% levels of  $T$ . For a given SEOS, maximum linearity and sensitivity are achieved by locating the Q-point  $\sim 1/4$  the distance between two adjacent isochrome minimums or maximums. Not only may the Q-point be shifted within the LIF, but the LIF-SEOS separation distance may also be increased or decreased, and the Q-point relocated. As the LIF-SEOS separation increases, the LIF

expands according to the LIF divergence index,  $\alpha_s$ .  $\delta V$  increases and  $I$  decreases, resulting in decreased sensitivity.  $I$  may be increased to compensate, but crystal limitations (e.g. optical damage) may limit the maximum  $I$ . Sensitivity may also be increased by choosing EO materials with large values of  $\eta_j$ .

#### High-Frequency (HF) BW Considerations:

If  $(\partial E_i / \partial t)_{\max} < \tau_d$ , where  $\tau_d$  is the maximum transit time of sensing light through the crystal, BW is limited by the continuum of eigenmodes that exist within the SEOS. Only a sub-continuum of eigenmodes pass through  $\Sigma$ , and one of those eigenmodes (BW-eigenmode) determines the AC BW ( $BW_{AC}$ ).<sup>19</sup> If  $(\partial E_i / \partial t)_{\max} < \tau_d$  is not true, BW will be insufficient. For HF  $\vec{E}_0$ ,  $BW_{AC} = ck/(n_s d)$ ,  $0 < k < 1$ , where  $c \approx 3 \times 10^8$  m/sec,  $d$  is the distance traversed through the SEOS by the BW-eigenmode,  $n_s$  is the slow index of refraction, and  $k$  is the fraction of a full cycle of  $\vec{E}_0$  that occurs during  $\tau_d$ . A conservative value of  $k$  is 0.1. Since  $n_e = n_e(\lambda, \vec{E})$  and  $n_o = n_o(\lambda, \vec{E})$ , BW may also be increased by choosing values of  $\lambda$  that result in small values of the larger of  $n_e$  and  $n_o$ . For a naturally birefringent SEOS, where  $n_e = n_e(T)$  and  $n_o = n_o(T)$ , and  $T$  is temperature,  $BW = BW(T)$ . For sensors with conductive components, stray reactances limit BW to  $< 1$  GHz.<sup>20</sup>

#### Proof-of-Principle Experiment for LIF Measurement of High-Voltage and $\vec{E}$ Pulses Demonstrated Using a LiNbO<sub>3</sub> SEOS

##### Description of the Experiment:

The experimental layout is shown in Fig. (2). The SEOS is used

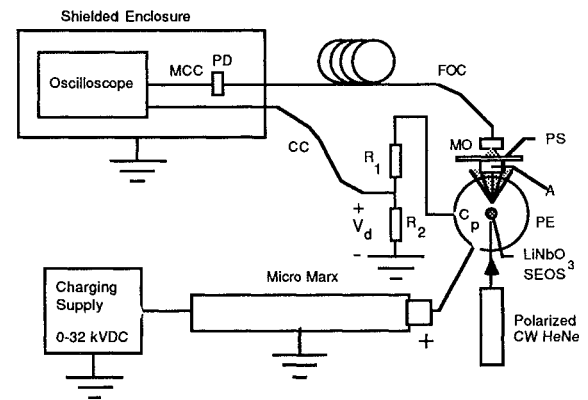


Fig. (2) Schematic of experiment. The  $\mathcal{P}$ -state of the HeNe (20 mW) was oriented at  $\sim 45^\circ$  to the vertical in order to obtain a brighter LIF. FOC: fiber optic cable; A: analyzer; PS: projection screen; MO: microscope objective; MCC: microwave coaxial cable; PD: photodetector; CC: coaxial cable; PE: plate electrode of parallel plate capacitor  $C_p$ . A top view of the laser, parallel plate capacitor, analyzer, and MO arrangement is shown. The micro-Marx and the resistive divider ( $R_1$  and  $R_2$ ) are connected to the upper plate of  $C_p$ . The upper plate is shown transparent, and exactly covers the lower plate.

measure the voltage across and the  $\vec{E}$  of  $C_p$ .  $V_d$  is a reference measurement.  $C_p$  was made of two horizontally parallel, aluminum plates ( $\sim 35$  cm. diam., separated by  $\sim 4$  cm of room air and two Lucite spacers that occupy  $\sim 9.5\%$  of the total plate area). In order to measure  $V_d$ , the LiNbO<sub>3</sub> SEOS was positioned between the two plates of  $C_p$ . A multimode FOC (50  $\mu$ m core; 10.59 m length), was run from the HV/EMI region and permanently attached to a PD. The MO effectively reduces the size of the LIF, and the SEOS response depends on the relative size of the MO image relative to the core diameter. The analyzing film, A, was crossed with respect to the HeNe. The HV output of a micro-Marx<sup>26</sup> was connected to the top plate to produce a uniform peak  $\vec{E}$  of  $\sim 1.5$  MVm<sup>-1</sup> -  $\sim 2.5$  MVm<sup>-1</sup> between the plates. The bottom plate was grounded.

#### A LiNbO<sub>3</sub> SEOS:

A proof-of-principle SEOS is made from a solid LiNbO<sub>3</sub> sphere. A large sensitivity was desired for the experiment in hope to observe a nonlinear SEOS response and measure  $V_{\pi}$ . The SEOS orientation was achieved using 360° LIF<sup>8</sup> images as a guide (Fig. 3). The a and b axes were left arbitrarily oriented. The LiNbO<sub>3</sub> SEOS and support stand are

DIAMETER:  $\sim 3$  mm  
 SPHERICITY:  $6.35 - 12.7 \times 10^{-7}$   
 SURFACE FLATNESS:  $0.5 - 1 \lambda$   
 (632.8 nm)  
 SCRATCH/DIG:  $5 - 5 <$   
 $n_o = 2.286$   $n_e = 2.200$  (632.8 nm)  
 $\rho = 5 \times 10^{-8}$  (400 C) ohm-cm  
 $\epsilon_{11}^S = \epsilon_{22}^S = 43$ ,  $\epsilon_{33}^S = 28$   
 $\alpha_s = 0.12 \text{ cm}^{-1}$

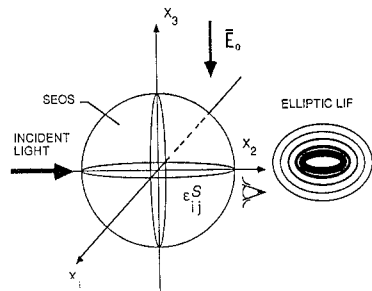


Fig. 3. Characteristics and orientation of LiNbO<sub>3</sub> SEOS. The SEOS orientation was chosen to achieve a low value of  $V_{\pi}^6$  ( $\vec{E}_0 = \vec{0}$  when orienting the sphere).  $x_3$  is the c-axis, and  $x_2$  is an axis normal to the plane containing the c-axis and an axis normal to the c-axis. The LIF is observed by projecting onto a screen.

shown in (Fig. 4).

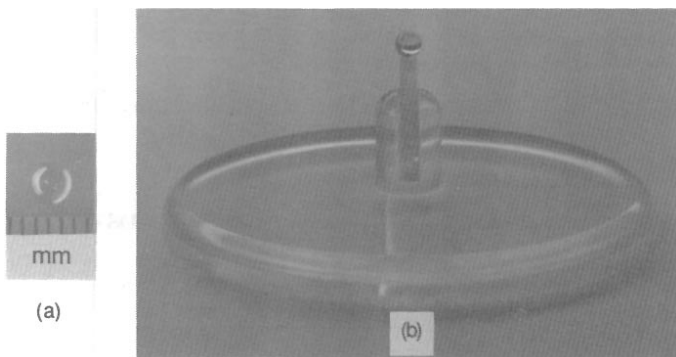


Fig. 4. LiNbO<sub>3</sub> SEOS (a) and LiNbO<sub>3</sub> SEOS on Lucite HV stand (b).

#### Calibration of the SEOS:

Calibration takes place in two steps. First, optical calibration is necessary when selecting a Q-point. The micro-Marx is disconnected from  $C_p$ , and a source (100 kV power transformer) of 60 Hz sinusoidally alternating HV (an easily detected, steady-state, low frequency measurand of known characteristics) is connected in series with  $C_p$  and  $R_1 + R_2$ . The SEOS response for any Q-point may be continuously monitored while changes in the position of  $\Sigma$  relative to the LIF are made in order to locate the linear and non-linear regions of the LIF pattern. Once, the desired 60 Hz AC response has been found, the 60 Hz HV source is disconnected, and the micro-Marx is reconnected without disturbing the SEOS or the MO-FOC assembly. A sinusoidal  $\vec{E}$  of  $\sim 125 \text{ kV m}^{-1}$  to  $\sim 575 \text{ kV m}^{-1}$  peak was used to calibrate the Q-points. Second, amplitude calibration is achieved from a reference signal using a conventional measurement technique. A photograph of the measurement and calibration system is shown in Fig. 5.

#### Experimental Results:

SEOS response to HV pulses were observed for different Q-points (Fig. 6). Time constants,  $\tau$ 's, associated with the SEOS rise and fall times and the divider fall time were consistent having average values of:  $\tau_{\text{rSEOS}} = 0.099 \text{ msec}$ ,  $\tau_{\text{fSEOS}} = 0.610 \text{ msec}$ ,  $\tau_{\text{divider}} = 0.62 \text{ msec}$ . The light and dark pulse responses of the SEOS are consistent with the Q-points, and the convergence of the elliptic isochromes to the point of intersection of the major and minor axes. Nonlinear Q-points B and D resulted in a reduced amplitude of the SEOS signal, as compared to more linear A and C responses. Spurious voltage spikes appear in the  $V_d$  signals. For B, the SEOS has responded to one of the downward spikes. A small amplitude light pulse with an exponential decay occurred from the SEOS in response to the initial  $V_d$  pulse. At the time of the spike, the SEOS again responded with a smaller amplitude light pulse that decayed exponentially, suggesting that perhaps the micro-Marx shorted and then re-erected. A similar behaviour is noted for the dark pulse of D. Slight SEOS responses to positive spurious pulses are shown for A, C, and D. Positions B and D were easily and accurately located using the AC calibration procedure, while positions A and C were not. For static field conditions, several quantities may be determined using the isotropic sphere approximation in the limits as  $r \rightarrow \pm d/2$  with  $\phi = \theta = 0$ , and  $\vec{E}_0$  parallel to

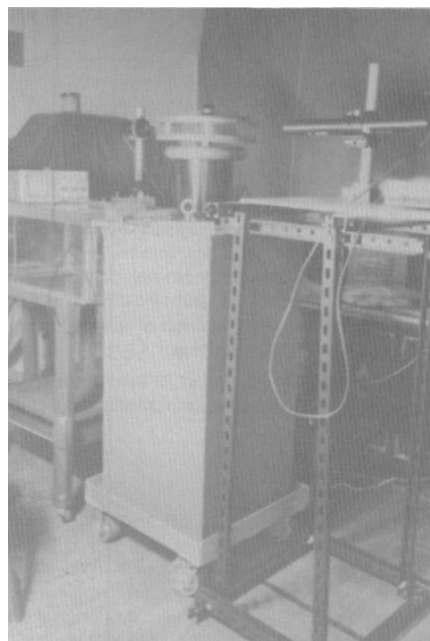


Fig. 5. Measurement and calibration system. The 100 kV AC transformer serves the dual purpose of providing a 60 Hz HVAC sinusoidal calibration voltage, and support of  $C_p$  for pulsed HV measurements. The micro-Marx is not shown.

$\langle r=1, \phi=0, \theta=0 \rangle$ , in spherical coordinates. Approximate ranges of the maximum experimental values of  $E_i$ ,  $E_e$ , and  $\Delta V$  applied to the LiNbO<sub>3</sub> SEOS are:  $0.15 < E_{i\text{max}} < 0.25 \text{ MV m}^{-1}$ ,  $4.2 < E_{e\text{max}} < 7.0 \text{ MV m}^{-1}$ , and  $0.45 < \Delta V_{\text{max}} < 0.75 \text{ kV}$ , respectively.  $V_{\pi}$  is estimated to be  $\sim 375 \text{ kV}$ .  $(dT/dV)_{\text{max}} \approx 4.2 \times 10^{-6} \text{ V}^{-1}$ .  $V_{\pi}$  was neither measured nor detected.  $\vec{E}$ -enhancement ( $\beta$ )<sup>23</sup> and efficiency ( $\eta$ )<sup>27</sup> are:  $\beta = (\eta)^{-1} \approx 2.8$ .  $\vec{E}_{0\text{max}}$  is determined by the  $\epsilon$ - $E_D$  product. With  $E_{be} \approx 3 \times 10^6 \text{ V m}^{-1}$  and  $E_{bi} > E_{be}$ , the maximum static voltage across  $C_p$  is limited to  $\sim 43 \text{ kV}$ . The SEOS remains uniaxial, and  $n_o^S(\vec{E}) > n_e^S(\vec{E})$  for all  $|\vec{E}| > 538 \text{ MV m}^{-1}$  in the chosen configuration, based on the HF index ellipsoid. Since the Q-point was not located at the intersection of the major and minor axes of the elliptic isochromes, the rays passing through  $\Sigma$  propagated a distance  $< d$  through the SEOS. The o-ray limit is:  $BW_{AC} > 4.38 \text{ GHz}$ . Less conservative values of  $k=0.25$  and  $0.5$  yield  $10.9 \text{ GHz}$  and  $21.9 \text{ GHz}$ , respectively. Planned future improvements of this experiment should provide better correlation between the SEOS signal and another type of conventional non-EO signal.

As one final illustration of the usefulness and appropriateness of EO sensors for HV measurement in space, a comparison of the UTA/CECR SEOS and another conventional non-EO HV probe is made in Fig. 7.

#### Acknowledgements

This work is sponsored by the Strategic Defense Initiative Office of Innovative Science and Technology through Defense Nuclear Agency Contract No. DNA001-85-C-0181. We are very grateful to Jimm Thomas of Deltronic Crystal Industries for providing the LiNbO<sub>3</sub> sphere and sphere parameters, Dr. Burke Burkart, University of Texas at Arlington Geology Dept., for helpful discussions about IFs and use of petrographic microscope facilities, and to Dr. K. W. Chen, Center for Accelerator Science and Technology, University of Texas at Arlington, for providing the 100 kV transformer. We would also like to thank R. Edwards, M. K. Browder, T. Pickens, and Dr. K. W. Reed for providing equipment and useful discussions. The references listed are not complete, and are only a few examples of the many efforts that have been made in the area of EO sensing.

#### References

1. M. C. McKinley, MSEE thesis, University of Texas at Arlington, Arlington, Texas, 1989.
2. M. C. McKinley, C. V. Smith, Jr., W. C. Nunnally, and R. Magnusson, "Design Considerations for a Fiber Optic High-Voltage Measurement System (HVMS) with Applications to Space Environments", *Bull. Am. Phys. Soc.*, vol. 33, p. 1482, July/August 1988.
3. S. Namba, "High Voltage Measurement by ADP Crystal Plate", *Rev. Sci. Instrum.*, vol. 27, p. 336, 1956.

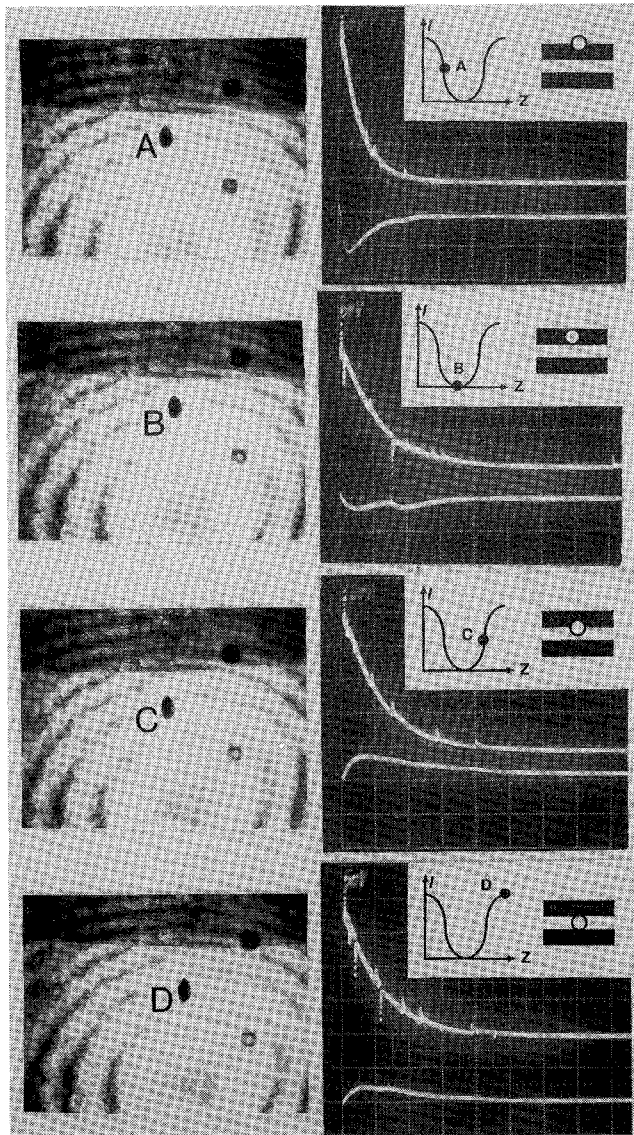


Fig. 6. Elliptic LIFs of a  $\text{LiNbO}_3$  SEOS,  $V_d$  (upper waveform), and corresponding SEOS response (lower waveform) to pulsed micro-Marx  $\bar{E}_0$ . The MO aperture is the small dark oval just above the center of the LIF photographs, and the letters A,B,C,D relate the MO aperture position to the isochrome  $I$  profile (inset). The two dark spots to the right of the MO aperture are screw heads used to attach the PS and A to the MO-FOC coupler. The dark rectangular region at the top of each LIF photograph is the shadow of the upper plate of  $C_p$ . The LIF in the shadow is a LIF reflection from the lower plate of  $C_p$ . MO aperture positions shown are not the actual positions present at the time the signals were recorded, but were photographed after the response measurements were taken, and accurately represent the actual MO aperture positions at the time the measurements were made (the LIF did not change). The amplitude scale is 1 V/div for all  $V_d$  waveforms (corresponds to  $|\bar{E}_0| = 500 \text{ kV/m}^2/\text{div}$ ), and 5 mV/div (A,B,D) and 10 mV/div (C) for the SEOS signal. The SEOS signals are uncalibrated in amplitude. The time scale is 500  $\mu\text{sec}/\text{div}$  (B,C,D) and 1 msec/div (A).  $I$  is increasing downward for all SEOS signals.

- <sup>4</sup>S. Namba, "High Voltage Measurement by ADP Crystal Plate", *Rev. Sci. Instrum.*, vol. 32, No. 5, pp. 595-597, May 1961.
- <sup>5</sup>E. G. Ehlers, *Optical Mineralogy*. Blackwell Scientific Publications, 1987.
- <sup>6</sup>P. V. Lenzo, E. G. Spencer, and K. Nassau, "Electro-Optic Coefficients in Single-Domain Ferroelectric Lithium Niobate", *J. Opt. Soc. Am.*, vol. 56, pp. 633-635, May 1966.
- <sup>7</sup>M. C. McKinley, C. V. Smith, Jr., W. C. Nunnally, R. Magnusson and T. D. Black, "Design Considerations for Electro-Optic High-Voltage (HV) Sensors", *Bull. Am. Phys. Soc.*, vol. 34, p. 1511, June, 1989.
- <sup>8</sup>M. C. McKinley, C. V. Smith, Jr., W. C. Nunnally, R. Magnusson, and T. D. Black, "A New Technique for Producing Laser Interference Figures (LIFs) of Crystals", *Bull. Am. Phys. Soc.*, vol. 34, p. 1511, June, 1989.

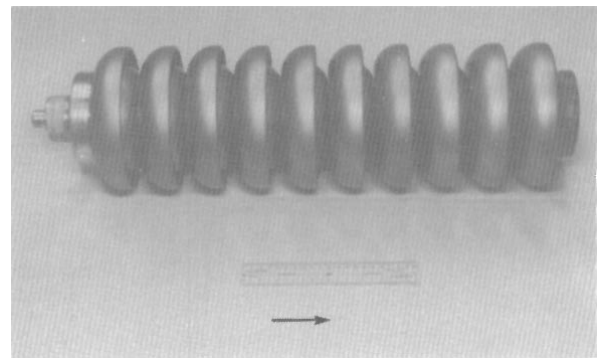


Fig. 7. Comparison of UTA/CECR mockup of the Westinghouse SPEAR II IV probe (above 20 cm ruler), and the UTA/CECR  $\text{LiNbO}_3$  SEOS (below the ruler, indicated by arrow).

- <sup>9</sup>M. Kanoi, G. Takahashi, T. Sato, M. Higaki, E. Mori, and K. Okumura, "Optical Voltage and Current Measuring System for Electric Systems", *IEEE Trans. Power Delivery*, vol. PWRD-1, pp. 91-97, Jan. 1986.
- <sup>10</sup>T. Mitsui, K. Hosoe, H. Usami and S. Miyamoto, "Development of Fiber-Optic Voltage Sensors and Magnetic-Field Sensors", *IEEE Trans. Power Delivery*, vol. PWRD-2, pp. 87-93, Jan. 1987.
- <sup>11</sup>G. A. Massey, D. C. Erickson, and R. A. Kadlec, "Electromagnetic Field Components: Their Measurement Using Linear Electrooptic and Magneto-optic Effects", *Appl. Opt.*, vol. 14, pp. 2712-2719, Nov. 1975.
- <sup>12</sup>H. M. Hertz and P. Thomsen, "Optical Wideband High-Voltage Measurement System", *Rev. Sci. Instrum.*, vol. 58, pp. 1660-1664, Sept. 1987.
- <sup>13</sup>H. Trinks, G. Matz, and H. Schilling, "Electro-Optical System for EMP Measurement", *IEEE Trans. on Electromagn. Compat.*, vol. EMC-22, pp. Feb. 1980.
- <sup>14</sup>K. D. Masterson, "Photonic Electric-Field Probe for Frequencies Up to 2 GHz", *SPIE Vol. 720 High Bandwidth Analog Applications of Photonics*, pp. 100-104, 1986.
- <sup>15</sup>T. Sasano, "Laser CT and Laser PD for EHV Power Transmission Lines", *Electrical Engineering in Japan*, vol. 93, pp. 91-98, 1973.
- <sup>16</sup>Y. Hamasaki, H. Gotoh, M. Katoh, and S. Takeuchi, "OPSEF: An Optical Sensor for Measurement of High Electric Field Intensity", *Electron. Lett.*, vol. 16, pp. 406-407, May 1980.
- <sup>17</sup>K. Hidaka, and Y. Murooka, "Electric Field Measurements in Long Gap Discharge Using Pockels Device", *Proc. IEE*, vol. 132, Pt. A, pp. 139-146, May 1985.
- <sup>18</sup>T. Kawamura, T. Matsumoto, M. Ishii, and T. Hisada, "Evaluation of Space-Charge Behaviour in Long Airgap Using Pockels' Cells", *Proc. IEE*, vol. 133, Pt. A, pp. 573-576, Nov. 1986.
- <sup>19</sup>B. N. Nelson, C. Menzel, and T. G. DiGiuseppe, "Fiber Optic Electric Field Sensor Configurations for High Bandwidth Lightning Research Measurement Applications", *SPIE Vol. 720 High Bandwidth Analog Applications of Photonics*, pp. 85-90, 1986.
- <sup>20</sup>J. Chang, C. N. Vittitoe, B. T. Neyer, and W. P. Ballard, "An Electro-optical Technique for Intense Microwave Measurements", *J. Appl. Phys.*, vol. 57, pp. 4843-4848, June 1985.
- <sup>21</sup>K. Hidaka and T. Kouno, "A Method for Measuring Electric Fields in Space Charge by Means of Pockels Device", *J. Electrostat.*, vol. 11, pp. 195-211, 1982.
- <sup>22</sup>S. R. M. Robertson and A. J. Rogers, "Measurement of DC Electric Fields Using the Electro-Optic Effect", *Proc. IEE*, vol. 132, pp. 195-198 1985, June.
- <sup>23</sup>R. V. Latham, *High Voltage Vacuum Insulation: The Physical Basis*. ©1981 Academic Press Inc. (London) Ltd., ch. 3, p. 57.
- <sup>24</sup>B. D. Popovic, *Introductory Engineering Electromagnetics*, ©1971 by Addison-Wesley Publishing Company, Inc., ch. 4, p. 160.
- <sup>25</sup>A. Yariv and P. Yeh, *Optical Waves in Crystals*, ©1984 by John Wiley & Sons, Inc., ch.7, p. 241.
- <sup>26</sup>D. A. Platts, "10 Joule High Voltage Trigger Micro Marx", *Digest of Technical Papers, 3rd IEEE International Pulsed Power Conference*, Albuquerque, New Mexico, June 1-3, 1981, pp. 485-486.
- <sup>27</sup>E. Kuffel and W. S. Zaengl, *High-Voltage Engineering Fundamentals*. ©1984 E. Kuffel and W. S. Zaengl, Pergamon Press, p. 210.